




# Structural, Thermal and Magnetic Characterization of Polycrystalline Ni-Mn-Ga Ferromagnetic Shape Memory Alloys

K. V. Batista<sup>a\*</sup> , J. M. Quirino<sup>a</sup>, C. R. Souto<sup>a</sup>, F. R. Feitosa<sup>a</sup>, R. M. Gomes<sup>a</sup>, B. Guedes<sup>a</sup> ,  
F. W. E. L. A. Júnior<sup>a</sup> 

<sup>a</sup>Universidade Federal da Paraíba, João Pessoa, PB, Brasil.

Received: April 13, 2023; Revised: October 01, 2023; Accepted: October 20, 2023

Shape memory alloys (SMA) are now widely studied in academia and have increasing usage in industry, as they allow efficient performance compared to mechanic actuators with reduced dimensions and the possibility of sensing temperature through the material itself. A subclass of the SMAs are the alloys with magnetic shape memory, still little explored as intelligent materials in Brazil. They combine the best properties of SMAs and common magnetostrictive materials. The magnetic shape memory alloys (MSMA) can be activated not only by the presence of a thermal stimulus, but also by the presence of an applied magnetic field. In this research, the polycrystalline magnetic shape memory alloys  $\text{Ni}_{51.3}\text{Mn}_{24}\text{Ga}_{24.7}$  and  $\text{Ni}_{54}\text{Mn}_{21}\text{Ga}_{25}$  were manufactured and characterized. Differential scanning calorimetry, X-Ray diffraction, energy dispersive X-ray spectrometry and scanning electron microscopy analyzes were performed to thermoanalytically and crystallographically characterize the alloys. Magnetic characterizations were also performed using Magnetic force microscopy. The results of the characterizations showed that the production process and the heat treatment were satisfactory for the fabrication of the ferromagnetic polycrystalline alloys. Besides that, the compositions  $\text{Ni}_{51.3}\text{Mn}_{24}\text{Ga}_{24.7}$  and  $\text{Ni}_{54}\text{Mn}_{21}\text{Ga}_{25}$  presented austenitic and martensitic 5M structures, respectively, at room temperature and it was possible to observe the alignment of the magnetic domains after magnetization.

**Keywords:** *Magnetic shape memory alloy, Ni-Mn-Ga, Heusler alloys, NiMnGa polycrystals.*

## 1. Introduction

The discovery of Heusler alloys at the beginning of the 20th century had a considerable impact on the field of magnetism. Scientific development on Heusler alloys has shown the great versatility that this new class of compounds offers. Alloys in this category have attracted attention due to their important characteristics such as magnetic shape memory effect, magnetocaloric effect, and large magnetoresistance effect<sup>1-3</sup>. During the past two decades, intensive attention has been devoted to these multifunctional alloys due to their great potential for applications in magnetic sensing, actuation and magnetic refrigeration<sup>4</sup>.

Magnetic shape memory properties are the best known features of Heusler alloys. The large deformations of these alloys are achieved by reorientation of martensitic variants in which the twin boundaries are highly mobile. This reorientation can be produced by stress and/or the application of a magnetic field. The complex behavior exhibited by these materials is a consequence of the strong coupling between magnetism and the structure which is driven by the martensitic transition<sup>1,5,6</sup>.

Ferromagnetic shape memory alloys (FSMA) or magnetic shape memory alloys (MSMA) combine the best properties of shape memory alloy (SMA) and common magnetostrictive materials. These alloys not only exhibit a relevant shape memory effect but can also be used in completely new

applications, given their complex mechanical behavior. These alloys demonstrate significant strain (from 6% to 12%) under an external magnetic field, which combined with their wide actuation frequency range, rapid accelerations, and high energy efficiency has resulted in MSMAs being used in a wide range of applications, for example, for energy harvesting, in measurement devices, flow control and local deformation for a miniaturized peristaltic pump to adjustable dosing, and as actuators and mechanical vibration damping<sup>7,8</sup>.

Ni-Mn-Ga alloys are a new class of active materials, and show giant magnetic field-induced strain (MFIS). They are potential materials both for sensors and actuators due to their unique microstructure and crystalline phases at various temperatures<sup>9</sup>. MFIS in this alloy was first observed experimentally by Ullakko et al.<sup>10</sup>, a MFIS of 0.2% in single crystalline  $\text{Ni}_2\text{MnGa}$  alloy was reported. It is possible to develop large reversible magnetic field induced strain when, in response to magnetic field induced stress, the crystallographic domains of the martensitic phase are rearranged. Until now large MFIS at room temperature was demonstrated so far only for Ni-Mn-Ga<sup>11</sup>.

An understanding of the microstructure and crystal structure associated with the transformation of austenite into martensite is important, as the properties of Ni-Mn-Ga alloys are extremely sensitive to composition change<sup>12,13</sup>. Heusler alloys are mainly prepared as single-crystalline or polycrystalline bulk materials or thin films<sup>14</sup>. However,

\*e-mail: [kalineufcg@gmail.com](mailto:kalineufcg@gmail.com)

properties and phase transformation mechanisms are altered when scaling the bulk materials down to the nanoscale, potentially allowing to modulate the main properties of Heusler alloys observed in bulk form and to tune their properties to be incorporated into new devices<sup>11</sup>.

The magnetic field strain is mainly presents in Ni-Mn-Ga single crystals, but the preparation of textured single crystal alloys is very complex for large scale applications, has a high cost, and is generally difficult due to the severe segregation of chemical composition that is unfavorable for obtaining stable functional properties<sup>15</sup>. In comparison, the preparation of polycrystalline alloys has lower cost and is much easier to obtain homogeneous chemical composition. The induced deformation due to magnetic field or by stress depends on the grain size, crystal structure and crystallographic orientation of Ni-Mn-Ga alloys, thus MFIS in polycrystalline Ni-Mn-Ga alloys are usually small because of random grain orientations and restriction of grain boundaries<sup>16-18</sup>.

Magnetic shape memory alloys are a new and rapidly developing class of smart materials<sup>8</sup>, with special attention to the Ni-Mn-Ga family alloys. For the most part, the research aims to quantify the deformations given a magnetic field applied to an alloy of a given composition, to mechanically and magnetically characterize these alloys, and to apply it as an actuator, often linear. Predominantly, research related to magnetic shape memory is done abroad, with a small amount of Brazilian research, and with a focus on single crystals. In Brazil, thin films grown on substrates have been the most widely used configuration for magnetic shape memory effect alloys in research. This work aims to contribute to the development of magnetic shape memory research in Brazil, by manufacturing polycrystalline Ni-Mn-Ga alloys with dimensions compatible with applications in sensors and actuators. This paper investigated the structural, thermal and magnetic characterization of polycrystalline Ni-Mn-Ga alloys for validation of the production process.

## 2. Materials and Methods

The polycrystalline ingots were produced by melting in a cold crucible induction furnace. A vacuum of up to  $10^{-3}$  m bar was created inside the chamber and flushed with high pure argon gas before the melting process. During melting, the chamber was completely filled with argon gas. High purity raw materials were weighed in stoichiometric ratio. After the first melt, all the ingots are reverted and submitted to a second melt under argon atmosphere. This melting procedure

was repeated up to 2 times to ensure a good homogeneity in the sample (Figure 1a). The total mass of the samples after casting was approximately 10 grams.

Heat treatment was carried out at a temperature of 800 °C for 40 hours to homogenize the samples. The cooling process was carried out inside the oven until room temperature. The samples were cut into parallelepiped shapes by electroerosion (Figure 1c). Table 1 shows the two nominal compositions of the Ni-Mn-Ga polycrystals obtained.

X-Ray Diffraction (XRD) pattern was used to study the structure of the prepared samples, a Bruker model D2 phaser diffractometer was used. The radiation used was  $\text{CuK}\alpha$  and all analyzes were carried out at room temperature in a range of incidence angles  $2\theta$  from 10° to 90°. For each phase, the unit cell parameters and atomic coordinates were determined by the Rietveld method using the TOPAS software version 4.2 and database inorganic crystal structure database (ICSD) for to completely identify crystal structures. Scanning electron microscopy (SEM) in front side of the samples (Figure 1d) was performed to identify the microstructure. Energy Dispersive X-ray Spectrometry (EDS) was used to characterization of chemical elements in the sample using a SEM model Mira 3 TESCAN.

The different transformations and their evolution after annealing were examined by means of differential scanning calorimetry (DSC) at heating/cooling rates in the range 10°C/min, a Shimadzu DSC-60 was used. The analysis was performed under nitrogen atmosphere at a flow rate of 50 ml/min over a temperature range of -30 °C to 120 °C, at a rate of for all analyses.

Magnetic force microscopy (MFM) was used to observe magnetic domains using a Shimadzu model SPM-9600. To analyze the orientation of the magnetic domains in front side of the sample (Figure 1d), the samples were subjected to magnetic fields of three intensities. Initially, each sample was magnetized for one minute and after analysis of the magnetic domains, the samples were demagnetized for one minute and subjected to a higher intensity field and the

**Table 1.** Nominal compositions (at %) of the Ni-Mn-Ga alloys used in this work for the characterization studies.

Sample name	Nominal composition (%)		
	Ni	Mn	Ga
Sample Polycrystalline 1	54	21	25
Sample Polycrystalline 2	51.3	24	24.7

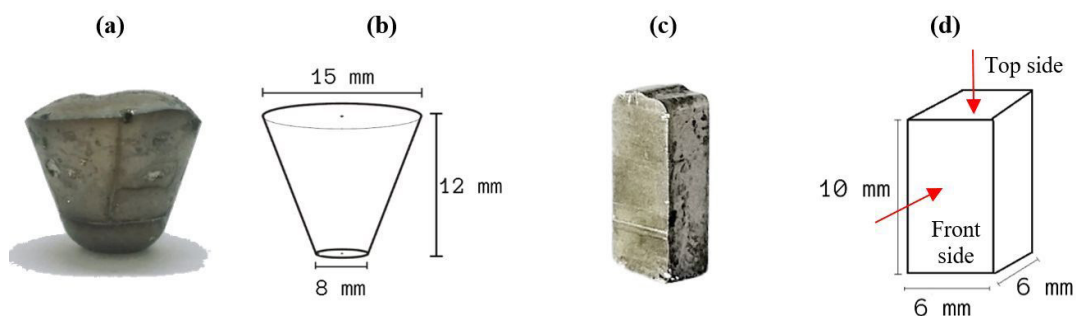


**Figure 1.** Dimensions of the polycrystalline sample melted and after cut for analysis.

magnetic domains were analyzed again. The samples were magnetized with magnets with fields of about 150 mT, 400 mT and 650 mT. The residual magnetic field value in the samples was measured with a Tunkia TD8620 gaussimeter immediately after the magnetizations and demagnetizations.

### 3. Results and Discussion

#### 3.1. Structural and microstructural characterization

XRD analyses at the polycrystalline alloys were performed in order to study the effects of the processing on the crystalline structure of the material, adjustment by Rietveld refinement of the XRD patterns collected from an polycrystalline 1 and 2 samples are reported in Figure 2. Table 2 presents data on the crystallographic properties of the polycrystalline samples.

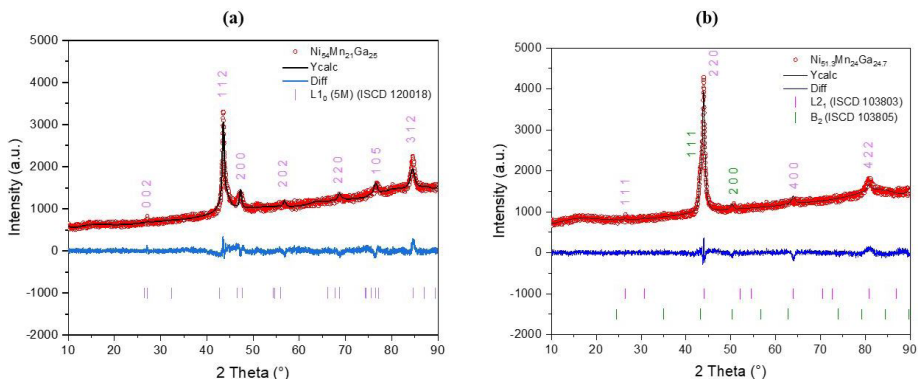
In Figure 2a peaks of highest intensity are observed at  $2\theta$  values of  $43.558^\circ$  with a second at  $84.519^\circ$  with 69% of the intensity value of the first. The diffraction planes in the pattern for alloy shows a single tetragonal martensite phase identified as  $L1_0$  with structural five-layered martensite (5M), space group  $I4mm$  and lattice parameter  $a = 0.39017$  nm and  $c = 0.65262$  nm. Jiang et al.<sup>19</sup> reports the same martensite crystal structure at room temperature by powder X-ray diffraction for alloy  $Ni_{54}Mn_{21}Ga_{25}$ .

Figure 2b where two peaks of higher intensity are visible, the first at a  $2\theta$  value of  $43.961^\circ$ , and the second at  $2\theta$  value of  $80.825^\circ$  with intensity at 25% of the previously mentioned peak. Peaks with intensities less than 1% were disregarded in the analysis. The reflection in the pattern for alloy is indexed to an austenite phase with  $L2_1$  cubic structure and a second phase with  $B2$  cubic structure. The ordered  $L2_1$  austenite structure with a lattice parameter close to 0.583 nm and  $Fm3m$  space group. The obtained value for the lattice parameter  $a = b = c = 0.5810$  nm is coincident with that reported in the literature (0.5825 nm)<sup>6,20,21</sup>. The Ni-Mn-Ga alloys solidify into a partially disordered intermediate  $B2$  phase at a certain composition-dependent temperature<sup>22</sup>. The identification of the disordered phase  $B2$  with  $Pm3m$  space group can be identified by XRD analysis or DSC peaks, this transformation is second order and the temperature of this transition decreases with Ni content<sup>23-25</sup>.

A morphological analysis was carried out through scanning electron microscopy observations on samples in order to evaluate the densification achieved by the microstructure evolution after the annealing processes. Figure 3 shows the images obtained at 250x and 500x amplification for the polycrystalline 1 sample. Polycrystalline grain boundaries and many lamellae with different orientations appear on the surface of the polycrystalline 1 sample, this structure identified by slats, spear or needles indicates the martensitic phase at room temperature characteristic of the Heuslers

**Table 2.** XRD parameters obtained from Rietveld refinements of sample polycrystalline 1 and 2.

Sample polycrystalline	Phase	Spacegroup	Lattice Parameters (Å)	Rwp	Rp	$\chi^2$	Atom (Wyck. Site)	Atomic coordinates		
								x	y	z
$Ni_{54}Mn_{21}Ga_{25}$	$L1_0$ (5M)	$I4/m m m$	$a = 3.9017(6)$ $c = 6.5262(9)$	4.82	3.59	1.57	Ni1 (4 d)	0.000	0.500	0.250
							Mn1 (2 b)	0.000	0.000	0.500
							Ni2 (2 b)	0.000	0.000	0.500
							Ga1 (2 a)	0.000	0.000	0.000
$Ni_{51.3}Mn_{24}Ga_{24.7}$	$L2_1$	$Fm-3m$	$a = 5.9273(6)$	3.58	2.79	1.21	Ga1 (4 a)	0.000	0.000	0.000
							Mn1 (4 b)	0.500	0.500	0.500
							Ni1 (8 c)	0.250	0.250	0.250
	$B_2$	$Pm-3m$	$a = 5.8152(5)$	Ga1 (1 a)	0.000	0.000	0.000			
				Mn1 (1 a)	0.000	0.000	0.000			
							Ni1 (3 c)	0.000	0.500	0.500



**Figure 2.** Rietveld refinement of diffraction patterns obtained for each sample recorded at ambient temperature: (a) Sample Polycrystalline 1 ( $Ni_{54}Mn_{21}Ga_{25}$ ); (b) Sample Polycrystalline 2 ( $Ni_{51.3}Mn_{24}Ga_{24.7}$ ).

alloys<sup>26</sup>. The regions indicated by the arrows correspond to internal twins are boundaries of martensite plate variants, which are so-called “variant accommodation twins”. The variant accommodation twin is introduced as a result of mutual accommodation of shear strains between variants in the martensite<sup>27</sup>. The arrangement of variants can occur on different length scales, from a few nanometers up to a few millimeters depending on grain size and processing. The martensitic variants consist of macro and micro twins with the fine lamellae being twin related with respect to the macro twins<sup>28</sup>. Similar observations on microstructure for the martensite phase of Heusler alloys were also reported by Pushin et al.<sup>29</sup> and Ma et al.<sup>30</sup>.

The chemical composition of polycrystalline sample 1 was determined using energy dispersive X-ray spectroscopy,  $\text{Ni}_{54.3}\text{Mn}_{21.6}\text{Ga}_{24.1}$ . The analysis of the EDS showed a uniform distribution of the elements nickel, manganese and gallium. Therefore, there are no significant changes in composition. A summary of the results including the average concentrations (out of twelve measured spots) and standard deviation is given in Figure 4. The average composition verified from the analyzed spots they have a satisfactory approximation to the nominal composition,  $\text{Ni}_{54}\text{Mn}_{21}\text{Ga}_{25}$ .

The results of scanning electron microscopy are reported in Figure 5 for the sample polycrystalline 2 obtained at 100x and 150x ampliation. The Figure 5 shows the grain boundaries of the polycrystalline sample with the presence of precipitates. A predominantly austenitic structure is observed according to the results presented by DRX and thermal analysis. Micrographs reported by Panda et al.<sup>31</sup> and Eto et al.<sup>32</sup> exhibit a similar morphology to ferromagnetic alloys in the austenitic phase. Using energy dispersive X-ray spectroscopy, the composition of the ingot was determined to be  $\text{Ni}_{51.3}\text{Mn}_{24.6}\text{Ga}_{24.1}$  for sample polycrystalline 2. The EDS mapping showed a uniform distribution of elements. The variation in manganese content was attributed to oxidation, due to the low vapor pressure of Mn, while the variation in gallium content can be attributed to the adhesion of the element in the alumina crucible. A summary of the results including the average concentrations (out of twelve measured spots) and standard deviation is given in Figure 6.

Figure 7 shows the results of the DSC measurements for the polycrystalline samples. The curve in Figure 7a showed low intensity peaks, at temperatures compatible with the literature for austenitic (A) and martensitic (M) transformation for this composition, at 56.77 °C on cooling and 84.73 °C on

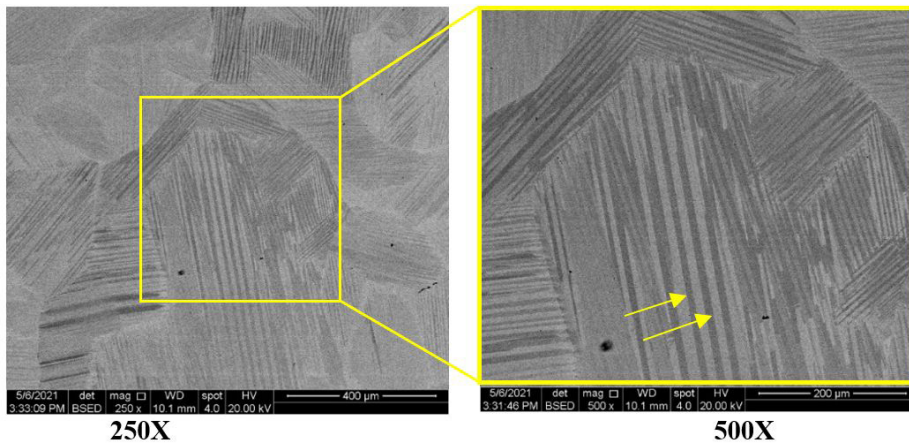
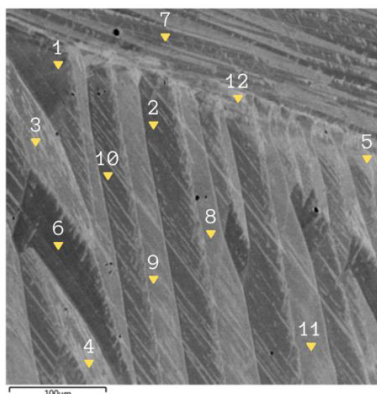


Figure 3. Scanning electron microscopy for sample Polycrystalline 1:  $\text{Ni}_{54}\text{Mn}_{21}\text{Ga}_{25}$ .



Selected area for EDS analysis	Ni (%)	Mn (%)	Ga (%)
Spot 1	54.4	21.8	23.8
Spot 2	54.3	21.7	23.9
Spot 3	54.5	21.3	24.2
Spot 4	54.4	21.4	24.2
Spot 5	54.2	21.1	24.7
Spot 6	54.2	22.1	23.8
Spot 7	54.6	21.6	23.8
Spot 8	54.4	21.1	24.6
Spot 9	54.6	21.2	24.2
Spot 10	54.5	21.9	23.6
Spot 11	54.2	21.5	24.3
Spot 12	54.5	21.4	24.1
<b>Average</b>	<b>54.4</b>	<b>21.5</b>	<b>24.1</b>
<b>Standard deviation</b>	<b>0.1</b>	<b>0.3</b>	<b>0.3</b>

Figure 4. Energy dispersive X-ray spectroscopy for Sample Polycrystalline 1.

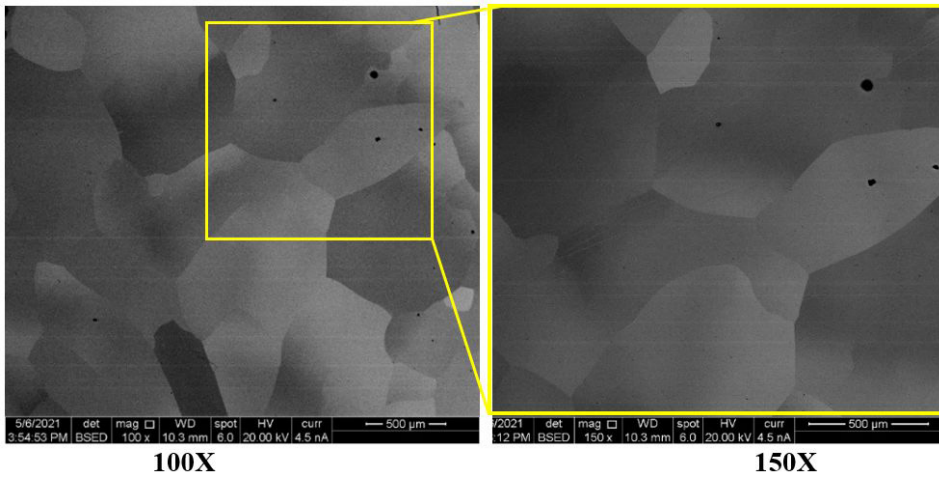
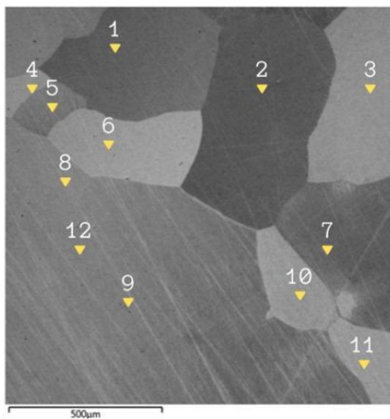


Figure 5. Scanning electron microscopy for sample Polycrystalline 2:  $\text{Ni}_{51.3}\text{Mn}_{24}\text{Ga}_{24.7}$ .



Selected area for EDS analysis	Ni (%)	Mn (%)	Ga (%)
Spot 1	50.8	25.1	24.1
Spot 2	51.4	24.3	24.3
Spot 3	51.3	24.5	24.2
Spot 4	51.3	24.5	24.2
Spot 5	51.2	24.2	24.6
Spot 6	50.8	24.4	24.8
Spot 7	51.3	24.4	24.3
Spot 8	51.0	24.4	24.6
Spot 9	51.1	24.7	24.2
Spot 10	51.3	24.4	24.3
Spot 11	51.1	24.3	24.6
Spot 12	51.6	24.3	24.1
<b>Average</b>	<b>51.2</b>	<b>24.5</b>	<b>24.3</b>
<b>Standard deviation</b>	<b>0.2</b>	<b>0.2</b>	<b>0.2</b>

Figure 6. Energy dispersive X-ray spectroscopy for sample Polycrystalline 2.

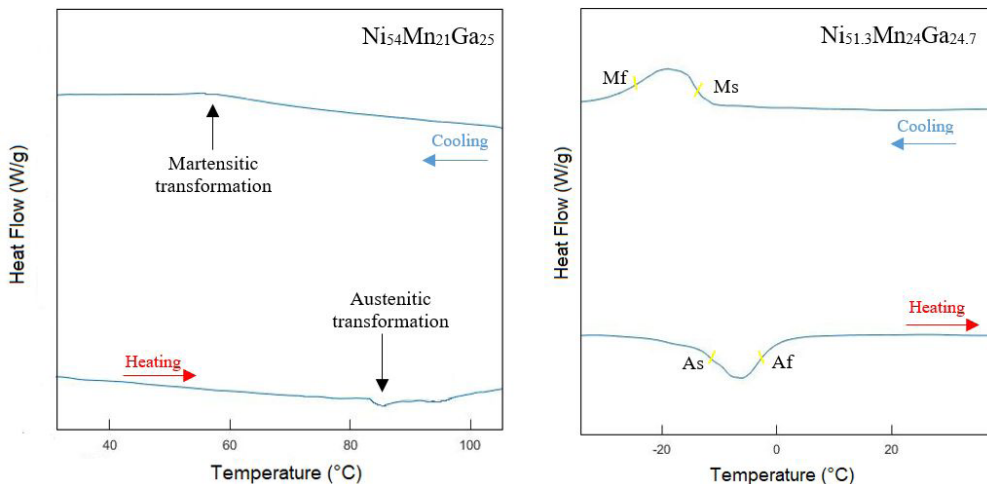


Figure 7. DSC (heat flow versus temperature) obtained for polycrystalline ingots: (a) Composition  $\text{Ni}_{54}\text{Mn}_{21}\text{Ga}_{25}$ ; (b) Composition  $\text{Ni}_{51.3}\text{Mn}_{24}\text{Ga}_{24.7}$ .

heating, respectively. Due to the low intensity of the peaks, it was not possible to identify the start and end temperatures of the transformations, only being possible to infer the average temperatures. The analysis of the curve presented in Figure 7b, identified the start temperature of the austenitic transformation (As) of  $-11.81^{\circ}\text{C}$  and final (Af) of  $-1.87^{\circ}\text{C}$  during heating, the cooling identified a start temperature of the martensitic transformation (Ms) of  $-12.73^{\circ}\text{C}$  and final (Mf) of  $-25.22^{\circ}\text{C}$ . Some studies report different phase transformation temperatures for the same compositions characterized in this study, as shown in the Table 3.

The transformation temperature of the martensitic phase in magnetic shape memory alloys strongly depends on the chemical composition<sup>6,35</sup>, but a comparison of experimental data from alloys with similar chemical composition shows that it is the processing methods and heat treatment parameters that influence the structural and magnetic properties of these alloys through changes in their microstructures, as seen in the data in the Table 3.

### 3.2. Magnetic characterization

Figure 8 and 9 shows the surface morphology and magnetic domains for polycrystalline sample 1 and sample 2 respectively. Images were photographed using magnetic force microscopy (MFM). In the MFM images, only the contrast of ripple were observed. Dark areas in the MFM image indicate that the “c” direction is perpendicular to the surface and the magnetic moment is going into the surface while bright areas correspond to the magnetic moment coming out of the surface as Müllner et al.<sup>36</sup> observed in monocrystalline samples in the martensitic phase. Similar magnetic domain structures were reported for tetragonal Ni–Mn–Ga martensite by Pan and James<sup>37</sup> and Ge et al.<sup>38</sup>. According to the domain contrast the magnetization direction could be easily determined<sup>38</sup>, which is indicated by the arrows in Figure 8c and 9c. The ripple contrast was gradually increased according to the magnetic field intensity for the

two polycrystalline samples, as shown in Figures 8 and 9. It can be seen that the alignment of the domains is larger and more visible as the magnetic field is stronger.

In Figure 8 it is noted that for the magnetization with the 150 mT and 400 mT magnets there are areas where the domains show small changes in direction. The visualization of the domains is dependent not only on the strength of the magnetic field applied to the sample but also on the region of analysis. Since it is necessary to remove the sample at each magnetization, it is not possible to fix the analyzed region. As a consequence, different results from those presented can be obtained when analyzing different regions. To get the best possible image, regions near the edges of the sample were chosen where the highest residual field was found, avoiding regions with visible defects or textures.

Figure 9 shows qualitative results of magnetic domains for polycrystalline sample 2. In the sample 2 it is possible to observe that the alignment of the domains is larger and more visible as the magnetic field is raised. It is noticeable that the domains have a greater thickness in orthogonal perspective (Figure 9b). The visualization of the 3D domains of the sample 2 after magnetization with a 650 mT magnet was the result with the highest visibility, although a linear pattern without deviations, expected for a sample magnetized with a high magnetic field, could not be visualized. The observed deviations can be explained by the surface irregularity and defects of the analyzed region, as well as by the choice of a region where the alignment of the domains was not complete.

The residual magnetic field values before and after magnetization with the three magnets used, for both samples, were measured. The values shown represent the maximums obtained after successive measurements. It was possible to observe that as the magnetic field to which the alloy was exposed increased, there was also an increase in the residual field. The sample 2 showed higher residual field values than the sample 1. Table 4 presents the residual magnetic field results.

**Table 3.** Phase transformation temperature for alloys  $\text{Ni}_{54}\text{Mn}_{21}\text{Ga}_{25}$  and  $\text{Ni}_{51.3}\text{Mn}_{24}\text{Ga}_{24.7}$  reported in the scientific community.

Sample composition	Processing methods	Ms ( $^{\circ}\text{C}$ )	Mf ( $^{\circ}\text{C}$ )	As ( $^{\circ}\text{C}$ )	Af ( $^{\circ}\text{C}$ )	Reference
$\text{Ni}_{54}\text{Mn}_{21}\text{Ga}_{25}$	As-cast alloy after annealing $800^{\circ}\text{C}$ for 40 h	56.7	-	84.7	-	Our study
$\text{Ni}_{54}\text{Mn}_{21}\text{Ga}_{25}$	As-cast alloy before annealing	42.0	7.0	42.0	68.0	Pushin et al. <sup>29</sup>
$\text{Ni}_{54}\text{Mn}_{21}\text{Ga}_{25}$	Ribbons after annealing	21.0	13.0	17.0	29.0	Pushin et al. <sup>29</sup>
$\text{Ni}_{54}\text{Mn}_{21}\text{Ga}_{25}$	As-cast alloy after annealing $900^{\circ}\text{C}$ for 50 h	41.0	28.0	39.5	44.0	Kuchin et al. <sup>33</sup>
$\text{Ni}_{51.3}\text{Mn}_{24}\text{Ga}_{24.7}$	As-cast alloy after annealing $800^{\circ}\text{C}$ for 40 h	-12.7	-25.2	-11.7	-1.8	Our study
$\text{Ni}_{51.3}\text{Mn}_{24}\text{Ga}_{24.7}$	As-cast alloy after annealing $800^{\circ}\text{C}$ for 72 h	-16.8	-29.9	-11.4	1.4	Bessegghini et al. <sup>34</sup>
$\text{Ni}_{51.3}\text{Mn}_{24}\text{Ga}_{24.7}$	As-cast alloy after annealing $800^{\circ}\text{C}$ for 168 h	-13.3	-27.1	-11.8	-2.0	Bessegghini et al. <sup>34</sup>

**Table 4.** Residual field before and after magnetization.

Samples	Magnet (mT)	Field before magnetization (mT)	Field after magnetization (mT)
Sample Polycrystalline 1	150	0.16	3.95
	400	0.32	4.01
	650	0.25	4.51
Sample Polycrystalline 2	150	0.47	1.10
	400	0.23	2.04
	650	0.30	2.81

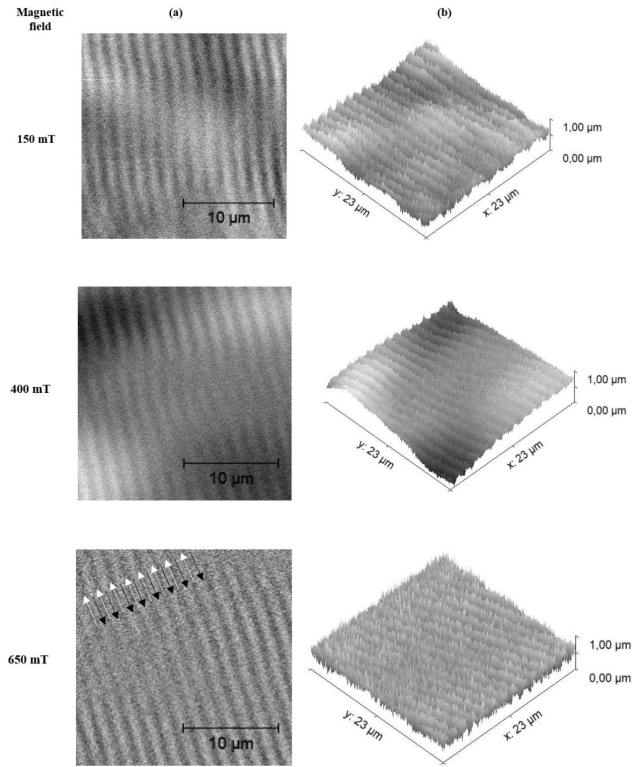


**Figure 8.** MFM images of the polycrystalline sample  $\text{Ni}_{54}\text{Mn}_{21}\text{Ga}_{25}$ : (a) Visualization of the magnetic domains after magnetization with a 150 mT, 400 mT and 650 mT; (b) 3D images of the topography of the polycrystalline sample  $\text{Ni}_{54}\text{Mn}_{21}\text{Ga}_{25}$  after magnetization with a 150 mT, 400 mT and 650 mT.

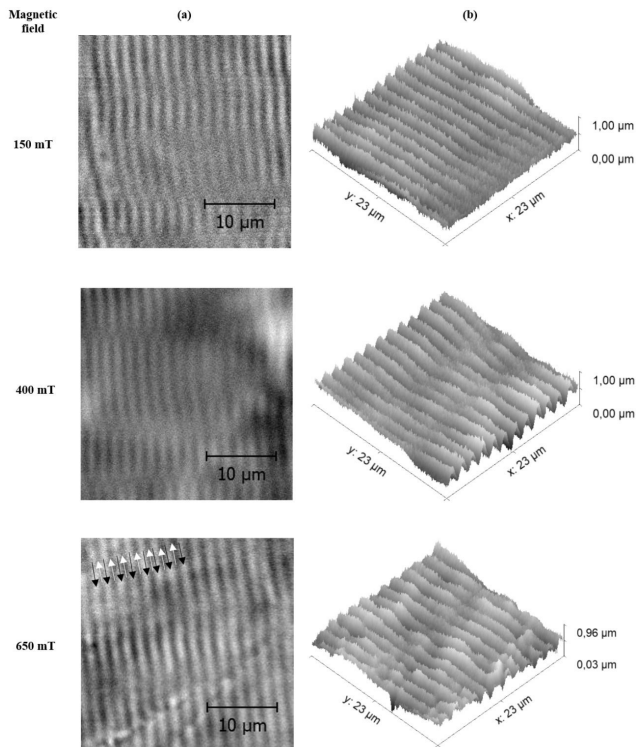


**Figure 9.** MFM images of the polycrystalline sample  $\text{Ni}_{51.3}\text{Mn}_{24}\text{Ga}_{24.7}$ : (a) Visualization of the magnetic domains after magnetization with a magnet 150 mT, 400 mT and 650 mT; (b) 3D images of the topography of the polycrystalline sample  $\text{Ni}_{51.3}\text{Mn}_{24}\text{Ga}_{24.7}$  after magnetization with a magnet 150 mT, 400 mT and 650 mT.

## 4. Conclusions

In this research, two ferromagnetic polycrystalline alloys were developed, in two compositions,  $\text{Ni}_{51.3}\text{Mn}_{24}\text{Ga}_{24.7}$  and  $\text{Ni}_{54}\text{Mn}_{21}\text{Ga}_{25}$ , and thermal, crystal structure and magnetic characterizations were performed on the polycrystalline samples.

The characterizations performed proved the expected properties in the alloys, such as crystalline structure at room temperature and martensitic transformation, consolidating the manufacturing method and treatments adopted. The compositions  $\text{Ni}_{54.3}\text{Mn}_{21.6}\text{Ga}_{24.1}$  for sample polycrystalline 1 and  $\text{Ni}_{51.3}\text{Mn}_{24.6}\text{Ga}_{24.1}$  for sample polycrystalline 2 presented martensitic 5M structures and austenitic, respectively, at room temperature.

The qualitative analysis of the magnetic domains of the polycrystalline samples using the MFM technique showed that a better alignment of the magnetic domains was observed when the samples were subjected to the highest intensity magnetic field (650 mT). No block walls and the geometry of the magnetic domains were observed in the areas covered by the experiment, potentially due to equipment limitations or domain size. Future research is needed to determine more data on the magnetic behavior of polycrystalline alloys.

## 5. Acknowledgments

This study was financed in part by the Coordenação de Aperfeiçoamento de Pessoal de Nível Superior (CAPES). The authors would like to thank the Conselho Nacional de Desenvolvimento Científico e Tecnológico (CNPq, Brazil) for supporting this work.

## 6. References

- Acet M, Mañosa L, Planes A. Magnetic-field-induced effects in martensitic heusler-based magnetic shape memory alloys in martensitic heusler-based magnetic shape memory alloys. In: Buschow KHJ, editor. Handbook of magnetic materials. Amsterdam: Elsevier. p. 231-89. (vol. 19).
- Dal S, Demirel B, Eskil M. The effects of homogenization time on the crystal structure and hardness of NiMnGaMo alloy. *Eng Sci Technol Int J*. 2020;24(4):1.
- Nambiar S, Murthy BRN, Sharma S, Prasanna AA. Martensitic transformation and magnetic properties of Ni-Mn Quinary Heusler alloy. *J. Compos. Sci.* 2023;7(1):1.
- Huang L, Cong D, Wang M, Wang Y. Coexisting multiple martensites in  $\text{Ni}_{57-x}\text{Mn}_{21-x}\text{Ga}_{22}$  ferromagnetic shape memory alloys: crystal structure and phase transition. *Metals*. 2021;81(6):467-9.
- Maji C. Properties of magnetic shape memory alloys in martensitic phase. *Curr Sci*. 2017;112(7):1390-401.
- Ullakko K, Ezer Y, Sozinov A, Kimmel G, Yakovenko P, Lindroos VK. Magnetic-field-induced strains in polycrystalline Ni-Mn-Ga at room temperature. *Scr Mater*. 2001;44(3):475-80.
- Ge Y. The crystal and magnetic microstructure of ni-Mn-Ga alloys. Helsinki: Helsinki University of Technology, 2014.
- Kulagin I, Li M, Laitinen V, Handroos H. Review of MSM actuators: applications, challenges, and potential. *IEEE Access*. 2022;10:83841-50.
- Javed K, Zhang XM, Parajuli S, Ali SS, Ahmad N, Shah SA, et al. Magnetization behavior of NiMnGa alloy nanowires prepared by DC electrodeposition. *J Magn Magn Mater*. 2020;498:166232.
- Ullakko K, Huang JK, Kantner C, O'Handley RC, Kokorin VV. Large magnetic-field-induced strains in  $\text{Ni}_2\text{MnGa}$  single crystals. *Appl Phys Lett*. 1996;69(13):1966-8.
- Zhang YC, Qin FX, Estevez D, Franco V, Peng HX. Structure, magnetic and magnetocaloric properties of  $\text{Ni}_2\text{MnGa}$  Heusler alloy nanowires. *J Magn Magn Mater*. 2020;513:167100.
- Zhou L, Schneider MM, Giri A, Cho K, Sohn Y. Microstructural and crystallographic characteristics of modulated martensite, non-modulated martensite, and pre-martensitic tweed austenite in Ni-Mn-Ga alloys. *Acta Mater*. 2017;134:93-103.
- Lanska N, Söderberg O, Sozinov A, Ge Y, Ullakko K, Lindroos VK. Composition and temperature dependence of the crystal structure of Ni-Mn-Ga alloys. *J Appl Phys*. 2004;95(12):8074-8.
- Dunand DC, Müllner P. Size effects on magnetic actuation in Ni-Mn-Ga shape-memory alloys. *Adv Mater*. 2011;23(2):216-32.
- Schlagel DL, Wu YL, Zhang W, Lograsso TA. Chemical segregation during bulk single crystal preparation of Ni-Mn-Ga ferromagnetic shape memory alloys. *J Alloys Compd*. 2000;312(1-2):77-85.
- Kumar AS, Ramudu M, Seshubai V. The role of quenched-in disorder in polycrystalline bulk and melt-spun ribbons of  $\text{Ni}_{50}\text{Mn}_{29}\text{Ga}_{21}$ . *Phase Transit*. 2021;94(3-4):183-91.
- Liao X, Xu X, Gao L, Khan MT, Hao C, Cheng F, et al. Influence of annealing on the damping behavior of Ni-Cu-Mn-Ga ferromagnetic shape memory alloys. *Materials*. 2020;13(2):480.
- Satpathy DK, Biswas S, Aich S. Microstructure and microtexture evolution in rapidly solidified melt-spun  $\text{Ni}_{50}\text{Mn}_{28}\text{Ga}_{22}$  ribbons. *J Magn Magn Mater*. 2021;527:167784.
- Jiang C, Feng G, Gong S, Xu H. Effect of Ni excess on phase transformation temperatures of NiMnGa alloys. *Mater Sci Eng A*. 2003;342(1-2):231-5.
- Pons J, Chernenko VA, Santamarta R, Cesari E. Crystal structure of martensitic phases in  $\text{ni} \pm \text{mn} \pm \text{ga}$  shape memory alloys. *Acta Mater*. 2000;48(12):3027-38.
- Ma Y, Awaji S, Watanabe K, Matsumoto M, Kobayashi N. X-ray diffraction study of the structural phase transition of  $\text{Ni}_2\text{MnGa}$  alloys in high magnetic fields. *Solid State Commun*. 2000;113(12):671-6.
- Cong D. Study on crystallographic features of Ni-Mn-Ga ferromagnetic shape memory alloys. France: University of Metz and Northeastern University; 2018.
- Wedel C, Itagaki K. High-temperature phase relations in the ternary Ga-Mn-Ni system. *J Phase Equilibria*. 2001;22(3):324-30.
- Khovailo V, Takagi T, Vasilev AN, Miki H, Matsumoto M, Kainuma R. On order-disorder ( $L_2$ -B2) phase transition in Ni-Mn-Ga Heusler alloys. *Phys Status Solidi, A Appl Res*. 2002;183(2):19-21.
- Goryczka T, Gigla M, Morawiec H. Effect of quenching on martensitic transformation course in non-stoichiometric NiMnGa alloy. *Int J Appl Electromagn Mech*. 2006;23(1-2):81-8.
- Zhou L, Giri A, Cho K, Heinrich H, Majumdar BS, Sohn Y. Microstructural and crystallographic characterization of  $\text{Ni}_{2-x}\text{Mn}_{1-x}\text{Ga}$  Alloys ( $x = 0.14, 0.16, 0.19, 0.22, \text{ and } 0.24$ ) by transmission electron microscopy. *Metall Mater Trans E*. 2014;1(3):239-46.
- Nishida M, Hara T, Matsuda M, Ii S. Crystallography and morphology of various interfaces in Ti-Ni, Ti-Pd and Ni-Mn-Ga shape memory alloys. *Mater Sci Eng A*. 2008;481(1-2):18-27.
- Chulist R, Böhm A, Oertel C-G, Skrotzki W. Self-accommodation in polycrystalline 10M Ni-Mn-Ga martensite. *J Mater Sci*. 2014;49(11):3951-5.
- Pushin VG, Marchenkova EB, Korolev AV, Kourov NI, Belosludtseva ES, Pushin AV, et al. Magnetically controlled thermoelastic martensite transformations and properties of a fine-grained  $\text{Ni}_{54}\text{Mn}_{21}\text{Ga}_{25}$  alloy. *Phys Solid State*. 2017;59(7):1321-31.
- Ma Y, Jiang C, Li Y, Xu H, Wang C, Liu X. Study of  $\text{Ni}_{50-x}\text{Mn}_{25}\text{Ga}_{25-x}$  ( $x = 2-11$ ) as high-temperature shape-memory alloys. *Acta Mater*. 2007;55(5):1533-41.
- Panda AK, Ghosh M, Kumar A, Mitra A. Magnetic transitions and structure of a NiMnGa ferromagnetic shape memory alloy



- prepared by melt spinning technique. *J Magn Magn Mater*. 2008;320(17):116-20.
32. Eto T, Xu X, Ito T, Honda F, Li DX, Oomi G, et al. Martensitic and magnetic transitions in  $\text{Ni}_{2+x}\text{MnGa}_{1-x}$  ferromagnetic shape memory alloys. *J Alloys Compd*. 2021;871:1-10.
  33. Kuchin DS, Dilmieva ET, Koshkid'ko YS, Kamantsev AP, Koledov VV, Mashirov AV, et al. Direct measurement of shape memory effect for  $\text{Ni}_{34}\text{Mn}_{21}\text{Ga}_{25}$ ,  $\text{Ni}_{50}\text{Mn}_{41.2}\text{In}_{8.8}$  Heusler alloys in high magnetic field. *J Magn Magn Mater*. 2019;482:317-22.
  34. Besseghini S, Pasquale M, Passaretti F, Sciacca A, Villa E. NiMnGa polycrystalline magnetically activated shape memory alloy: a calorimetric investigation. *Scr Mater*. 2001;44(12):2681-7.
  35. Khan RAA, Ghomashchi R, Xie Z, Chen L. Ferromagnetic shape memory Heusler materials: synthesis, microstructure characterization and magnetostructural properties. *Materials (Basel)*. 2018;11(6):988.
  36. Müllner P, Clark Z, Kenoyer L, Knowlton WB, Kosterz G. Nanomechanics and magnetic structure of orthorhombic Ni-Mn-Ga martensite. *Mater Sci Eng A*. 2008;48(1-2):66-72.
  37. Pan Q, James RD. Micromagnetic study of  $\text{Ni}_2\text{MnGa}$  under applied field. *J Appl Phys*. 2000;87(9):4702-6.
  38. Ge Y, Heczko O, Söderberg O, Lindroos VK. Various magnetic domain structures in a Ni-Mn-Ga martensite exhibiting magnetic shape memory effect. *J Appl Phys*. 2004;96(4):2159-63.